A Push Recovery Strategy for a Passively Compliant Humanoid Robot using Decentralized LQR Controllers

Emmanouil Spyrakos-Papastavridis, Gustavo A. Medrano-Cerda, Nikos G. Tsagarakis,
Jian S. Dai and Darwin G. Caldwell

***Abstract*—This paper presents a control scheme that is directed towards the performance of push recovery on the compliant humanoid robot, COMAN. The novelty offered by this work is related to the use of a decentralized controller based on an initial Limited Quadratic Regulator (LQR) design on a humanoid robot in addition to the regulation of the actual joint positions instead of the motor positions. Moreover, the ankle-knee strategy is examined through the use of a compliant double inverted pendulum model. A key feature of the propounded approach lies in the controller's ability to regulate the system's inherently compliant dynamics through considering not only the motor-related variables but also those of the link-side, appearing after the passive compliant element. Consequently, this leads to a control method that is capable of stabilizing the robot by means of increasing the damping on the link, which is essential given the system's oscillatory behaviour once it has been perturbed.**

***Index Terms*—Humanoid, passive compliance, optimal control.**

I. Introduction

The challenge of controlling an inverted pendulum has been a common research topic for the past decades, due mainly to its model's compatibility with those of numerous practical systems, especially in the field of humanoid robotics. The complexity of the problem is related to the inherent instability of the system and hence the difficulty in devising efficient control algorithms. For the majority of humanoids, using an inverted pendulum model to describe their structures may retain an adequate degree of accuracy, especially as far as the center-of-mass (COM) position is concerned [1]. This however would be a very rough approximation when using COMAN (a passively compliant humanoid), since its mechanical structure is different to conventional stiff robots. Compliant humanoid robots can be more adept at stabilizing their structures when subjected to perturbations as well as to adapting to irregular terrain. However, the dynamics of the compliant humanoid robot differs fundamentally from that of stiff systems, while also giving rise to an under-actuated control problem. Thus, a compliant double inverted pendulum model is introduced and employed for the development of the control scheme in this paper. The use of optimal control techniques on compliant systems has been the topic of several research works.

In [2], an inverse optimal PID approach was employed on a 2 degree-of-freedom flexible robotic manipulator, while in [3] control and anti-control methods have been used for trajectory tracking of such systems. Moreover, neural network and linear regulator control of compliant joints has been proposed [4]. This paper extends the use of optimal control techniques to a humanoid composed of flexible joints and uses decentralized LQR controllers whose application on humanoids has not been reported thus far, to the authors' knowledge.

In particular, push recovery, online and offline stabilization and zero-moment point (ZMP) tracking and feedback are some of the active topics in humanoid research where the inverted pendulum has been successfully adopted.

In [1], [5] and [6] such models (or slightly modified versions) were employed in the development of walking algorithms and push recovery schemes respectively. The concept of the ZMP has been offered to the field through the work presented in [7] wherein the authors propose a point under the foot sole whose position defines the dynamic balance of a bipedal system.

The work in [8] presents strategies for balancing a biped robot in the vertical stance, while in [9] they considered the dynamic balance of a humanoid taking the whole system's dynamics into account. The work described in [10] on the other hand is predominantly concerned with gravity compensation to render the robot passive and the translation of ground reaction forces to joint torques, a method which dispenses with the need for calculating full-body dynamics. [11] focuses on a passivity-based approach. In [12], it was demonstrated how the monitoring and modification of the rate of change of angular momentum as both a stability criterion and control variable, can be used to balance a biped robot. Zero-moment point preview control schemes are a common choice for stabilization and have been introduced to the field through [13]. [14] describes the development of an online stabilizer that performs torque control on the feet to correct a ZMP-based trajectory. An alternative version of ZMP-based trajectory generation, using receding horizon control, was propounded in [15]. The topic of using a system identification approach to enhance the accuracy of the inverted pendulum model has also been considered [16]. This involves feedback

E. Spyrakos-Papastavridis (emmanouil.spyrakos@iit.it), G. Medrano-Cerda (gustavo.cerda@iit.it), N. Tsagarakis (nikos.tsagarakis@iit.it) and D. G. Caldwell (darwin.caldwell@iit.it) are with the Department of Advanced Robotics, Fondazione Istituto Italiano di Tecnologia (IIT), Genova 16163, Italy.

Jian S. Dai (jian.dai@kcl.ac.uk) is with the Centre for Robotics Research, King's College London, Strand, London, WC2R 2LS, UK.

of the ZMP position, a topic described in [17] and [18] whose work was extended to the field of stepping in the presence of external perturbations. This entailed the execution of a step in such a way or towards a certain position, so as to bring about stability to the system. This leads to the next topic of stepping where the work seen in [19] attempts to provide an answer to the question of 'when and where must a step be taken' to stabilize a given system, by introducing the flywheel model, an extension of the inverted pendulum which has also been adopted in the work presented in [20]. To this end, capture points are proposed and extended in [21]. These are regions on the terrain, in which a robot can take a step while still maintaining stability.

Another means of stabilizing a humanoid is the simpler ankle strategy, involving movement of the entire system about the ankle which has been studied in [1], [5] and [6] where the authors have utilized torque control of the ankles. The addition of a spring in the ankle has given rise to further studies carried out in [22]. Related studies in the field of biomechanics include the works presented in [23] and [24]. A natural extension to these schemes, namely the hip strategy, has been examined in [6] and [19]. Moreover, [6] and [19] describe how a humanoid can switch between various strategies, i.e. hip strategy, ankle strategy and stepping to ensure stability. Contrarily, this paper deals with the ankle-knee strategy as it is more suited to our particular task. Regarding the use of the arms to achieve balance recovery, the literature is not as extensive, although [24] is directly concerned with this matter. Moreover, [25] describes the use of contact force optimization techniques to ensure that a humanoid retains its balance when subjected to disturbances, while [26] proposes gain-scheduling methods for the same purpose. [27] propounds allowing the ZMP to move in close proximity to the foot edge instead of constraining it to residing within the foot centre.

The paper is structured as follows; section II introduces the system model, section III describes the joint control scheme, section IV reports on the stabilization strategy which is based on ZMP tracking, section V presents the experimental results and finally section VI addresses the conclusions.

II. SYSTEM MODEL

A. Hardware Configuration

The compliant humanoid COMAN is currently constituted of 15 DOF's while the mathematical model treats a simplified double pendulum form of the robot. A visual representation of the robot can be seen in Figure 1. Each ankle joint incorporates three position sensors (2 absolute and 1 relative) and one torque sensor. The robot is also equipped with 6-axis force/torque sensors located at the ankles. Additionally, the COMAN has a 3-axis rate gyro sensor and a 3-axis accelerometer, located at the pelvis. Regarding the main controller, it is an Intel Core 2 Duo 1.5 GHz dual processor with 3.0 GB of RAM, running on a 64-bit Windows 7 operating system. Data communication with the motor drivers is performed via a real-time Ethernet protocol.

A unique feature of the system arises from its possession of compliant joints which are embedded with series elastic actuators (SEA) [28]. There are currently four such joints on the COMAN [29], namely the two sagittal ankle and the two sagittal knee joints. This offers the robot several benefits such as an increased capability to reject disturbances, as well as terrain adaptability. There is however a compromise that has to inevitably be taken into account and this is related to the increased complexity of the system and its associated control scheme. This is owed to the presence of the physical elasticity which could give rise to oscillatory behaviour. Therefore, devising simple motor control techniques for such a system is usually not sufficient.

B. Dynamical Model

Figure 2 provides a schematic of the approximated model used to describe the robot's structure when assuming a double support stance. This double inverted pendulum considers the two lower legs as having a combined inertia I_1, while the components appearing above the knee joints, namely the two thighs, the two hip joints and the torso, are treated as a single inertia I_2. The latter assumption may be considered to be valid given that the pertinent joints have been locked using high PID gains. Moreover, Figure 2 illustrates the presence of the springs in the ankles. The reason for choosing this model instead of a single inverted pendulum, is related to the former's offering of a greater range of motion through the addition of the knee joint. As the compliant humanoid does not currently possess an upper-body module, the effect of using a hip strategy would not be as significant with respect to the stabilization of the system, due to the small mass/inertia of the body section above the hip joints, and was therefore omitted from this work. Tests using the ankle-knee strategy on a humanoid have been previously carried out only on simulation [30].

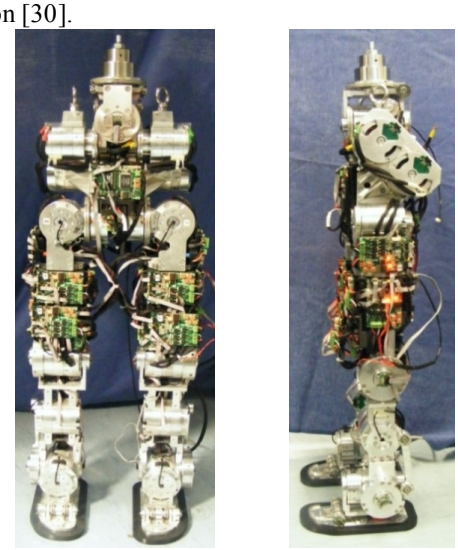

Fig.1. COMAN as viewed from the front (left) and from the side (right).

A representation of the dynamical model of the robot is offered by equation (1) below:

$$M\ddot{\theta} + N\dot{\theta} + P\theta = E_m\tau_m + E_d\tau \quad (1)$$

where M, N and $P \in R^{6x6}$ are the inertia, damping and stiffness matrices respectively, while $E_m \in R^{6x4}$ and $E_d \in R^{6x2}$ are the motor and joint torque selection matrices respectively. In a similar fashion, τ_m and τ represent the motor and joint torques matrices that can be expressed in the following way:

$$\tau_m = [\tau_{mla}\ \tau_{mra}\ \tau_{mlk}\ \tau_{mrk}]^T, \tau = [\tau_1\ \tau_2]^T$$

where $\tau_{mla}, \tau_{mra}, \tau_{mlk}$ and τ_{mrk} represent the left ankle, right ankle, left knee and right knee motor torques, whereas τ_1 and τ_2 denote the ankle and knee joint torques.
Additionally, in equation (1):

$$\theta = [\theta_1 \quad \theta_2 \quad \theta_{mla} \quad \theta_{mra} \quad \theta_{mlk} \quad \theta_{mrk}]^T$$

with θ_1 and θ_2 corresponding to the ankle and knee link positions, whereas θ_{mla}, θ_{mra}, θ_{mlk} and θ_{mrk} denote the motor positions. It has been demonstrated through equation (1) above, that the actuator models of both joints have been taken into account thus resulting in the creation of a compliant double inverted pendulum, which is introduced in this paper.

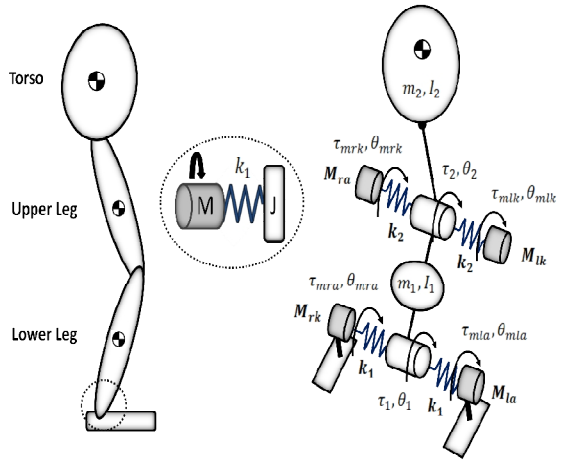

Fig.2. Schematic of the full COMAN model (left) and the compliant double inverted pendulum model (right), including the compliant actuation module.

TABLE I
MODEL PARAMETER VALUES

Parameter	Value
k_1	110 N/m
k_2	110 N/m
m_1	6.328 kg
m_2	11.088 kg
I_1	0.0122 kg m^2
I_2	0.1727 kg m^2

Therefore, this specific model only considers a double support stance and would require the inclusion of three additional link states to be rendered suitable for the representation of a single support configuration.

III. JOINT CONTROL

The control method employed for the purpose of regulating the joint-related states is based on an LQR scheme. The LQR controller proved to be an apt choice as it aimed at formulating an optimal relationship between the motor and link states. A similar approach to designing such controllers can be found in [31]. Furthermore, it is known that LQR controllers usually display good stability margins and robustness, as compared to other designs. Most importantly however, this control scheme exploits the system's natural dynamics, which is desirable in our case due to the robot's passively compliant structure, in addition to reducing the required control effort. The possession of an accurate mathematical model is a prerequisite for the existence of the above features. The dynamical model in (1) can be expressed in a compact state-space form which would then allow it to be readily exploited for LQR control.

$$\begin{bmatrix}\dot{\theta}\\ \ddot{\theta}\end{bmatrix} = \begin{bmatrix}0_{6X6} & I_{6X6}\\ -M^{-1}P & -M^{-1}N\end{bmatrix}\begin{bmatrix}\theta\\ \dot{\theta}\end{bmatrix} + \begin{bmatrix}0_{6X4}\\ M^{-1}E_m\end{bmatrix}V_m \quad (2)$$

in which $V_m = [V_{mla}\ V_{mra}\ V_{mlk}\ V_{mrk}]$ with $V_{mla}, V_{mra}, V_{mlk}$ and V_{mrk} symbolizing the control voltages. The more general LQR formulation of (2) is shown below:

$$\dot{\hat{x}} = \hat{A}\hat{x} + \hat{B}u, \quad \hat{y} = C\hat{x} \quad (3)$$

where $\hat{x}$ is the system state:

$$\hat{x} = [\theta_1\theta_2\theta_{mla}\theta_{mra}\theta_{mlk}\theta_{mrk}\dot{\theta}_1\dot{\theta}_2\dot{\theta}_{mla}\dot{\theta}_{mra}\dot{\theta}_{mlk}\dot{\theta}_{mrk}]^T$$

u is the control voltage input matrix and $C = [I_{6x6}\ 0]$. In order to improve the system's tracking performance, integral action was included on the link-side in the controller design, using:

$$\dot{z} = r - \hat{y} = r - C_1\hat{x} \quad (4)$$

where, $C_1 = [I_{2x2}\ 0_{2x10}]$. Thus, the continuous time tracking system is represented by the following equation:

$$\dot{x} = Ax + Bu + B_r r, \quad y = C_{cl}x + D_{cl}r \quad (5)$$

where,

$$x = \begin{bmatrix}\hat{x}\\ z\end{bmatrix}, A = \begin{bmatrix}\hat{A} & 0\\ -C_1 & 0\end{bmatrix}, B = \begin{bmatrix}\hat{B}\\ 0\end{bmatrix}, B_r = \begin{bmatrix}\hat{B}G_{ff}\\ I_{2x2}\end{bmatrix},$$
$$y = \begin{bmatrix}x\\ u\end{bmatrix}, C_{cl} = \begin{bmatrix}I_{14x14}\\ -K\end{bmatrix}, D_{cl} = \begin{bmatrix}0\\ G_{ff}\end{bmatrix},$$

where G_{ff} is the feed-forward gain and K is the state feedback gain matrix. The following two sub-sections describe the

procedure involved in the design of both the centralized and decentralized controllers.

A. Centralized Controller Design

This section presents the design of the centralized controller which served as a basis for the creation of the decentralized controller that is proposed in this paper.

The optimal feedback gain K is acquired by using the state feedback law $u = -Kx$ for the minimization of the cost function P, subject to the model's dynamics:

$$P = \int_0^\infty (x^T Q x + u^T R u) dt \tag{6}$$

The closed-loop system can therefore be computed as:

$$\dot{x} = A_{cl} x + B_r r \tag{7}$$

where $A_{cl} = A - BK$. In this scheme, since the integrator is applied on the link position, $G_{ff} = \alpha K[\,1\; 0_{1x10}]^T$, where $0 \leq \alpha \leq 1$. The feed-forward term is capable of speeding up the system's response without having an effect on the closed loop stability.

B. Decentralized Controller Design

Moving on to the description of the decentralized controller design, it must be reported that the main reason why it was developed was to allow for a design that would enable direct implementation on the DSP boards, which would offer faster controller responses. The method by which this decentralization was carried out involved the elimination of the coupling terms in the motor feedback. The described approach constitutes our proposed method of decentralization, and has not previously been applied to humanoids. Consequently, the LQR state feedback matrix K has the following structure:

$$K = \begin{bmatrix} K_1 & K_3 & K_{m1_{(1x4)}} & K_7 & K_9 & K_{m5_{(1x4)}} & K_{13} & K_{15} \\ K_1 & K_3 & K_{m2_{(1x4)}} & K_7 & K_9 & K_{m6_{(1x4)}} & K_{13} & K_{15} \\ K_4 & K_2 & K_{m3_{(1x4)}} & K_{10} & K_8 & K_{m7_{(1x4)}} & K_{16} & K_{14} \\ K_4 & K_2 & K_{m4_{(1x4)}} & K_{10} & K_8 & K_{m8_{(1x4)}} & K_{16} & K_{14} \end{bmatrix} \tag{8}$$

The decentralized feedback is then given by:

$$K = \begin{bmatrix} K_1\,0\,K_{m11}\,0\,0\,0\,K_7\,0\,K_{m51}\,0\,0\,0\,K_{13}\,0 \\ K_1\,0\,0\,K_{m22}\,0\,0\,K_7\,0\,0\,K_{m62}\,0\,0\,K_{13}\,0 \\ 0\,K_2\,0\,0\,K_{m33}\,0\,0\,K_8\,0\,0\,K_{m73}\,0\,0\,K_{14} \\ 0\;K_2\,0\,0\,0\,K_{m44}\,0\,K_8\,0\,0\,0\,K_{m84}\,0\,K_{14} \end{bmatrix} \tag{9}$$

Additionally, the Q and R penalties utilized in the design of the centralized controller were selected in such a way so as to yield a desired response time, while maintaining a small velocity gain magnitude due to the limitations imposed on the system by the relatively low encoder resolution (12-bit). There was also a need to retain the control voltage values below saturation levels. This meticulous tuning was mandatory since the decentralization was inevitably accompanied with a degradation in the performance, as compared to the centralized controller.

IV. EXPERIMENTAL SETUP

A. ZMP Tracking

To demonstrate the robustness of the controller described above, a push recovery stabilization task was performed while the robot was assuming a standing configuration. One of the most common methods used for the assessment of a humanoid's stability is the tracking of the zero-moment point, as has been described in the introduction section. Figure 3 presents a schematic that displays the CoM and ZMP positions with respect to the proposed double pendulum model. The force-torque sensors that are positioned at the soles of the robot's feet were exploited to obtain a measurement of the ZMP, through the relationship:

$$x_{ZMP} = -\frac{\tau_y}{F_z} \tag{10}$$

where τ_y is the y-axis torque, while F_z is the z-axis force.

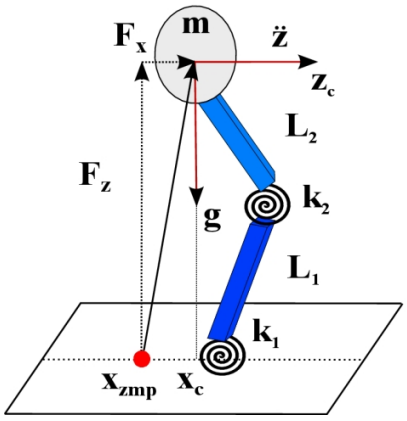

Fig.3. ZMP and CoM positions of the compliant double inverted pendulum.

Given the ZMP, it was then required to calculate the position at which the robot's centre-of-mass (COM) should be placed, in order to bring about stability to the system's structure. This was accomplished using:

$$x_C = \frac{F_x z_c}{F_z} + x_{ZMP} \tag{11}$$

where z_c is the fixed COM height and F_x is the x-axis force.. It can be seen that the above expression offers a mere approximation of x_C, as it considers z_c to be constant, which is only valid for small angles θ_1, θ_2. Once the desired COM position had been acquired, the joint reference angles were computed through the use of inverse kinematics. The generated joint reference angles were then fed as reference positions to the LQR controller.

B. Controller Specifications

Details of the values used in the controller tuning are given in the following lines, together with additional information associated to the simulation model. The first step in the development of the former was concerned with the discretization of the continuous form of the dynamical model, including the integrators, by using a sampling interval of $t_s = 1ms$. The choice of the sampling interval value was contingent upon the sampling time of the joints' DSP boards. Moreover, the link and motor velocities were computed through the averaging of a specific number of first order differences. The penalties used for the decentralized controller are the following:

$$Q = [.1\ .1\ .01\ .01\ .01\ .01\ 0\ 0\ 0\ 0\ 0\ 0\ 0\ .004\ \ 0.004]$$

$$R = [.1\ .1\ .1\ .1]$$

$$G_{ff} = 1.0\begin{bmatrix} K_1 & 0 \\ K_1 & 0 \\ 0 & K_2 \\ 0 & K_2 \end{bmatrix}, N_{av\_samples} = 15$$

One of the crucial criteria that was satisfied by the above penalties, was the prevention of the production of voltages that would exceed the saturation limit. The feed-forward gain was selected in such a way so as to minimize the overshoot of the response. Link position responses of 0.7 and 1 seconds were achieved for the knee and ankle joints respectively by using the above penalties that yielded a closed-loop bandwidth of 1.25 Hz for the ankle and 1.18 Hz for the knee.

V. RESULTS

A. Disturbance Application (Experiment 1)

A push recovery experiment was carried out to certify the robot's ability to recover from external perturbations generated through the application of impulsive strikes on the robot's structure using a metal pole. This can be seen in Figures 4 and 5, wherein the dotted lines signify the times at which the disturbances were applied to the system. Furthermore, the torso was pulled towards one direction for a specific time interval and then released, to confirm whether or not the integral action could cause instability when the pull magnitude was too large. Figure 4 also reveals the effects of static friction on the ankle joint through the motor's inability to respond to control voltages of magnitudes in the range of 0-0.8 Volts, in contrast to Figure 5, where the motor is constantly following the position of the link. Figure 6 justifies this discrepancy by illustrating the difference in the magnitudes of the control signals between the knee and ankle joints during Experiment 1, where it is evident that the knee is driven by significantly higher voltage levels.

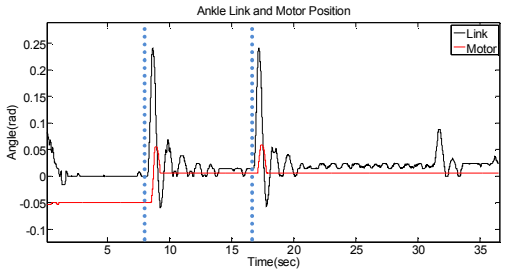

Fig. 4. Left ankle response when disturbed during Experiment 1.

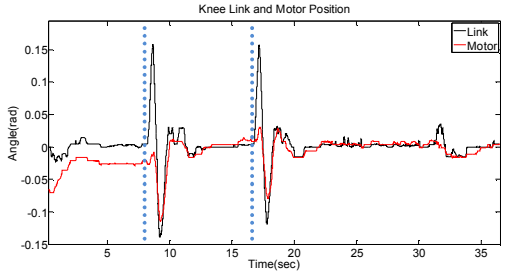

Fig. 5. Left knee response when disturbed during Experiment 1.

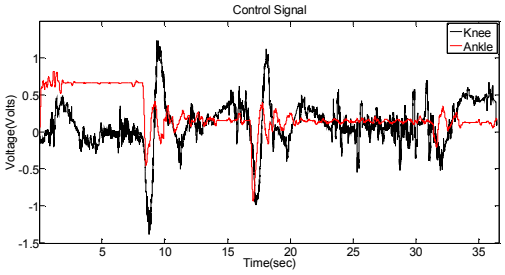

Fig.6. Control voltages produced during Experiment 1.

B. Load Addition (Experiment 2)

The experiments described in the subsequent lines involved the application of disturbances on the robotic structure while objects of varying weights had been placed onto the torso. It was desirable to demonstrate the robustness of the controller when subjected to deviations in the values of the system's mathematical model. A metal rod of 1.3 kilograms was attached onto the robot's torso while it was perturbed. The results of these trials can be observed in Figures 7 and 8.

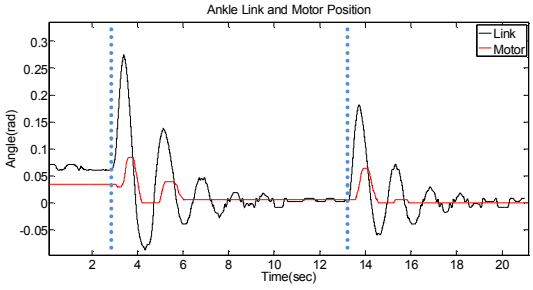

Fig.7. Left ankle response when disturbed during Experiment 2.

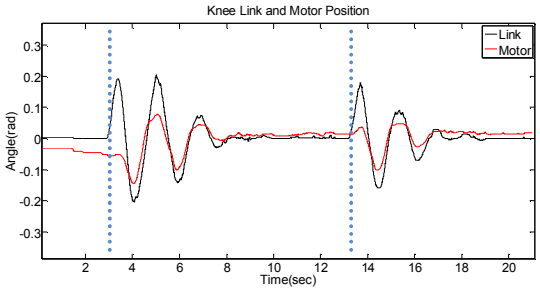

Fig.8. Left knee response when disturbed during Experiment 2.

C. Force Measurement (Experiment 3)

In order to measure the maximum force that could be applied to the system before it lost balance, a metal rod equipped with a force/torque sensor at its tip, was used to disturb the robot. The pertinent results are offered in Figures 9-12, where Figure 11 suggests that the robot is capable of recovering from impulses of 742 Newton seconds. The blue circles on the plots depict the instances at which balance could not be maintained. Furthermore, Figure 12 can provide information on the robot's stability, with the blue circles placed at the time instances where the ZMP position along the sagittal direction had a value of -6 for longer periods of time as compared to other instances on the plot. The value of -6 denotes the limit after which the robot was unable to recover its state of stability.

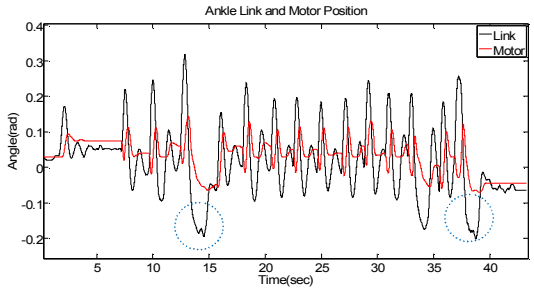

Fig.9. Left ankle response when disturbed during Experiment 3.

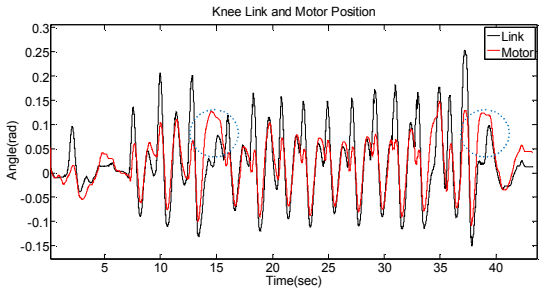

Fig.10. Left knee response when disturbed during Experiment 3.

D. Discussion

Observing Figures 4, 7 and 9, it can be seen that the motor responses are lagging with respect to the link responses, when a push has been applied to the system. This implies that the robot's inherent structural compliance absorbs the initial impact forces, while the motor action is activated at a later stage and attempts to minimize the system's oscillations and the steady state error. It is worth noting that the knee joint offers an improved response. The mentioned Figures also portray the differences in magnitudes between the link and motor responses, whilst maintaining a maximum deviation of 0.2 radians from one another, since this is the physically allowable limit of the series elastic actuators located at the compliant joints. It must be noted that the use of integral action on the link-side leads to a minimization of the passive compliance or to its complete elimination if perfect tracking is achieved and the gains are sufficiently high.

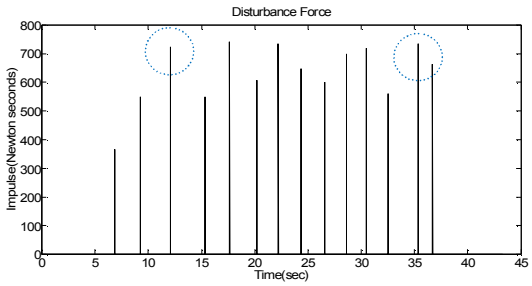

Fig.11. Impulses applied during Experiment 3.

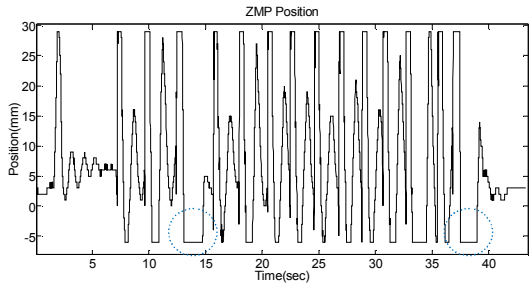

Fig.12. ZMP position along the z-axis during Experiment 3.

VI. CONCLUSIONS

It is concluded that the proposed controller was efficient in terms of offering the robot the capability of recovering from external disturbances, and hence LQR control proved to be a valid solution to this problem. This statement is confirmed through the results demonstrated in Figures 9-12 that reveal the controller's ability to reject disturbances of up to 742 Newton seconds while at the same time providing relatively fast responses, given the presence of the passive elastic elements. It may be argued that the suppression of the system's natural dynamics arising from the reduction of the passive compliance when performing link-side tracking, is counter-productive. This may be refuted by highlighting the need for accurate link-side tracking which could make the difference between successful and unsuccessful execution of a given trajectory. Therefore, an optimal strategy could be devised through the appropriate switching between compliant and 'stiff' modes during a desired trajectory. Aside from the

controller's performance however, it must be mentioned that the effectiveness of the passive compliance was crucial towards the attainment of our goal, as it aided in the handling of the impact forces. Nevertheless, the overall scheme could be expanded upon to allow for the rejection of larger pushes. One means of achieving this would be to improve the response of the controller or otherwise by exploiting a greater number of joints for the task. Even so, there is a limit in the magnitude of the pushes beyond which the robot will be unable to recover using only standing strategies and this will require stepping action which shall be considered in future developments.

ACKNOWLEDGMENT

This work is supported by the European Commission FP7, "AMARSI" Project ICT-2009-4.

REFERENCES

[1] S. Kajita, K. Tani, "Study of Dynamic Biped Locomotion on Rugged Terrain," *Fifth International Conference on Advanced Robotics (ICAR), Vol. 1, pp. 741 – 746, Pisa, Italy, 1991.*

[2] T. Ha, J. Lee, J. Park, "Robust control by inverse optimal PID approach for flexible joint robot manipulator," *IEEE International Conference on Robotics and Biomimetics (ROBIO), pp. 336 – 341, Sanya, China, 2007.*

[3] M. Kandroodi, F. Farivar, M. Pedram, M. Shoorehdeli, "Variable structure control and anti-control of flexible joint manipulator with experimental validation," *IEEE International Conference on Mechatronics (ICM), pp. 294 – 299, Istanbul, Turkey, 2011.*

[4] Z. Jiang, S. Higaki, "Control of Flexible Joint Robot Manipulators Using a Combined Controller with Neural Network and Linear Regulator," *Journal of Systems and Control Engineering,* Vol. 225, No. 6, pp. 798-806, *2011.*

[5] S. Kajita, K. Yokoi, M. Saigo and K. Tanie "Balancing a Humanoid Robot Using Backdrive Concerned Torque Control and Direct Angular Momentum Feedback," *Proceedings of the IEEE International Conference on Robotics & Automation, Vol. 4, pp. 3376-3382, Seoul, South Korea, 2001.*

[6] B. Stephens, "Humanoid Push Recovery," *7th IEEE-RAS International Conference on Humanoid Robots, pp. 589-595, Pittsburgh, USA, 2007.*

[7] M. Vukobratovic, B. Borovac, "Zero-moment point – Thirty Five Years of its Life," *International Journal of Humanoid Robotics (IJHR), Vol. 1, No. 1, pp. 157-173, 2004.*

[8] H. Hemami, B. Wyman, "Modeling and Control of Constrained Dynamic Systems with Application to Biped Locomotion in the Frontal Plane," *IEEE Transactions on Automatic Control, Vol. 24, No. 4, pp. 526-535, 1979.*

[9] B. Stephens, C. Atkeson, "Dynamic Balance Force Control for Compliant Humanoid Robots," *IEEE/RSJ International Conference on Intelligent Robots and Systems (IROS), pp. 1248 – 1255, Taipei, Taiwan, 2010.*

[10] S. Hyon, J. Hale, G. Cheng, "Full-Body Compliant Human-Humanoid Interaction: Balancing in the Presence of Unknown External Forces," *IEEE Transactions on Robotics, Vol. 23, No. 5, pp. 884-898, 2007.*

[11] Y. Kim, B. Lee, J. Ryu, J. Kim, "Landing Force Control for Humanoid Robot by Time-Domain Passivity Approach," *IEEE Transactions on Robotics, Vol. 23, No. 6, pp. 1294-1301, 2007.*

[12] A. Goswami, V. Kallem, "Rate of change of angular momentum and balance maintenance of biped robots," *IEEE International Conference on Robotics and Automation (ICRA), Vol. 4, pp. 3785-3790, New Orleans, USA, 2004.*

[13] C. Azevedo, P. Poignet, B. Espiau, "Moving horizon control for biped robots without reference trajectory," *IEEE International Conference on Robotics and Automation (ICRA), Vol. 3, pp. 2762-2767, Washington, USA, 2002.*

[14] S. Kajita, M. Morisawa, K. Miura, S. Nakaoka, K. Harada, K. Kaneko, F. Kanehiro, K. Yokoi, "Biped Walking Stabilization Based on Linear Inverted Pendulum Tracking," *IEEE/RSJ International Conference on Intelligent Robots and Systems (IROS), pp. 4489 – 4496, Taipei, Taiwan, 2010.*

[15] P. Wieber, "Trajectory Free Linear Model Predictive Control for Stable Walking in the Presence of Strong Perturbations," *IEEE-RAS International Conference on Humanoid Robots, pp. 137 – 142, Genova, Italy, 2006.*

[16] W. Suleiman, F. Kanehiro, K. Miura, E. Yoshida, "Enhancing Zero Moment Point-Based Control Model: System Identification Approach," *Advanced Robotics, Vol. 25, No. 3, pp. 427-446, 2011.*

[17] Napoleon, S. Nakaura, M. Sampei, "Balance Control Analysis of Humanoid Robot based on ZMP Feedback Control," *IEEE/RSJ International Conference on Intelligent Robot and Systems (IROS), Vol. 3, pp. 2437-2442, Lausanne, Switzerland, 2002.*

[18] S. Ito, S. Amano, M. Sasaki, P. Kulvanit, "A ZMP feedback Control for Biped Balance and its Application to In-Place Lateral Stepping Motion," *Journal of Computers, Vol. 3, No. 8, 2008.*

[19] J. Pratt, J. Carff, S. Drakunov, A. Goswami, "Capture Point: A Step toward Humanoid Push Recovery," *IEEE-RAS International Conference on Humanoid Robots, pp. 200-207, Genova, Italy, 2006.*

[20] J. R. Rebula, F. Canas, J. E. Pratt, A. Goswami, "Learning Capture Points for Bipedal Push Recovery," *IEEE International Conference on Robotics and Automation (ICRA), pp. 1774, Pasadena, USA, 2008.*

[21] M. Kim, J. Ho Oh, "Posture Control of a Humanoid Robot with a Compliant Ankle Joint," *International Journal of Humanoid Robotics (IJHR), Vol. 7, No. 1, 2010.*

[22] A. Hansen, D. Childress, S. Miff, S. Gard, K. Mesplay, "The human ankle during walking: implications for design of biomimetic ankle prostheses," *Journal of Biomechanics, Vol. 37, No. 10, pp. 1467-1474, 2004.*

[23] K. Chen, "Standing Human – an Inverted Pendulum," *Latin American Journal of Physical Education, Vol. 2, No. 3, 2008.*

[24] M. Nakada, B. Allen, S. Morishima, D. Terzopoulos, "Learning Arm Motion Strategies for Balance Recovery of Humanoid Robots," *International Conference on Emerging Security Technologies (EST), pp. 165-170, Canterbury, UK, 2010.*

[25] C. Ott, M. A. Roa, G. Hirzinger, "Posture and balance control for biped robots based on contact force optimization," *IEEE-RAS International Conference on Humanoid Robots, pp. 26-33, Bled, Slovenia, 2011.*

[26] D. Xing, C. Atkeson, B. Stephens, "Gain scheduled control of perturbed standing balance", *IEEE/RSJ International Conference on Intelligent Robot and Systems (IROS), pp. 4063 - 4068, Taipei, Taiwan, 2010.*

[27] A. Kawamura, "Maintaining floor-foot contact of a biped robot by force constraint position control," *IEEE International Conference on Mechatronics (ICM), pp. 857 – 862, Istanbul, Turkey, 2011.*

[28] N. Tsagarakis, M. Laffranchi, B. Vanderborght, D. G. Caldwell, "A Compact Soft Actuator Unit for Small Scale Human Friendly Robots", *IEEE International Conference on Robotics and Automation Conference, (ICRA), Kobe, Japan, pp. 4356-4362, 2009.*

[29] N. Tsagarakis, Z. Li, J. Saglia, D. Caldwell, "The Design of the Lower Body of the Compliant Humanoid Robot "cCub"", *IEEE International Conference on Robotics and Automation Conference, (ICRA), pp. 2035-2040, Shanghai, China, 2011.*

[30] H. Ono, T. Sato, K. Ohnishi, "Balance recovery of ankle strategy: Using knee joint for biped robot", *International Symposium on Access Spaces (ISAS), pp. 236 – 241, Yokohama, Japan, 2011.*

[31] H. Dallali, G. Medrano-Cerda, M. Brown, "A Comparison of Multivariable & Decentralized Control Strategies for Robust Humanoid Walking," *UK Automatic Control Conference (UKACC), Coventry, UK, 2010.*